Improving magnetic plasma control for ITER

Samo Gerkšič[a], Gianmaria De Tommasi[b]

[a]*Jožef Stefan Institute, Jamova 39, Ljubljana, Slovenia*
[b]*Consorzio CREATE / Università di Napoli Federico II, Dipartimento di Ingegneria Elettrica e delle Tecnologie dell'informazione, Via Claudio 21, 80125, Napoli, Italy*

Several alternative plasma control schemes using the same plasma current and shape controller (SC) with different plasma vertical stabilisation (VS) controllers are explored, assessing their efficiency in the suppression of plasma shape transients after vertical displacement event (VDE) disturbances and their robustness to changes of the local dynamics. We attempt to decrease the settling time and the overshoot peaks while maintaining robustness to changes of local dynamics, by speeding up the controller response to disturbances. For VS, static output feedback (SOF) and linear-quadratic-Gaussian (LQG) control are considered. Both SOF and LQG are further augmented with an additional intermediate-level control loop that attempts to bring the system back to the origin after a VDE event faster than the SC normally does.

Keywords: tokamak control, plasma shape control, vertical stabilization system, optimal control.

1. Introduction

The challenge of magnetic shape control of unstable elongated plasma in tokamak fusion reactors is to maintain the prescribed plasma shape subject to large-scale disturbances, such as vertical displacement events (VDE), H-L transitions and edge localised mode (ELM) perturbations, and to considerable changes of local dynamics in different operating points [1,2].

The plasma current, position, and shape controller proposal for the ITER tokamak [3] is one state-of-the-art approach to magnetic plasma shape control. It comprises a cascade scheme with an inner vertical stabilization (VS) controller based on static output feedback (SOF) [4], which stabilizes vertical plasma velocity on a fast time-scale, and an outer plasma current and shape controller (SC), which controls the plasma current and the plasma-wall distances (gaps) on a slower time-scale.

In this work we explore several alternative plasma control schemes using the same SC [5] with different VS controllers, assessing the control system efficiency in the suppression of plasma shape transients after VDE disturbances and the robustness to changes of the local dynamics. The main hypothesis is that a faster but still robust response may be achievable by speeding up the controller response to disturbances, due to the open-loop unstable process dynamics.

Firstly, we consider the recently implemented LQG (linear-quadratic-Gaussian) controller [6], which is known to provide a faster response with the superconductive VS actuator.

The second approach is based on the observation that in the original scheme [3] the VS only controls the plasma centroid vertical velocity v_p to 0, while the plasma centroid vertical position z_p is brought back to the origin by the SC on a slower time scale. Here we introduce an additional intermediate-level z_p control loop that attempts to bring the system back to the origin faster than the SC does. The approach is inspired by the proportional-integral LQG VS controller for the MAST tokamak of Ovsyannikov et al. [7], which penalises z_p in addition to v_p. Alternatively, this may be achievable by an additional control loop from the superconductive VS current IVS3, similarly to the intermediate-level VS current (I_{FRFA}) control in the JET VS system [2] (in JET this is needed to prevent current saturation in the case of periodic disturbances such as ELM, and to limit the VS thermal load, which is not a requirement for the superconductive VS circuit of ITER), or by modifying the design of the SC.

The paper is organised as follows. In Section 2, the simulation setup is described. Section 3 briefly describes the SC. In section 4, four variants of the VS controller are shown. Section 5 presents and discusses the simulation results.

2. Simulation setup

The simulations and controller design methods are based on high-order local linear dynamical models of the tokamak plasma from CREATE-L or CREATE-NL [8,9], at several different equilibrium points, defined by the nominal plasma current I_p, poloidal beta β_p, internal inductance l_i, elongation κ, and triangularity δ for the anticipated ITER plasma. The models used are listed in Table 1. Table 1 also reports if a given equilibrium corresponds to H mode or L mode plasma, while all the considered equilibria refer to diverted plasmas. The models have more than 100 states, representing the currents in the plasma, in the active conductors, and in the passive structures.

Table 1. Local linear dynamic models.

Model	I_p (MA)	β_p	l_i	κ	δ	H mode
LMVS	14.5	0.11	0.85	1.84	0.20	No
LMNE	15.0	0.10	1.21	1.85	0.49	No
LM52	15.0	0.10	0.80	1.86	0.49	No
LM53	15.0	0.10	1.00	1.87	0.50	No
LM59	15.0	0.60	0.60	1.93	0.47	Yes
LM60	15.0	0.60	0.80	1.86	0.48	Yes

The simulations were carried out using a Matlab/Simulink simulation scheme comprising:
- the plasma/circuits linearized model,

author's email: samo.gerksic@ijs.si

- a simplified model of plasma diagnostics for the plasma vertical velocity v_p and position z_p (a first-order dynamic lag filter with the time constant equal to $7 \cdot 10^{-3}$ s is considered),
- simplified models of the power supplies for the superconductive coils VS1 and for the in-vessel ohmic coils VS3 (a first-order dynamic lag with the time constant equal to $7.5 \cdot 10^{-3}$ s; a delay equal to $2.5 \cdot 10^{-3}$ s; saturations ±6 kV and ±1.5 kV for VS1 and VS3, respectively),
- simplified models of the main power supplies (saturations ±1.5 kV, except for VCS1 ±3 kV, and first-order dynamic lag with the time constant equal to 0.015 s and a delay equal to 0.015 s),
- the inner cascade control loop of the VS system, which aims at vertically stabilizing the plasma column,
- the outer cascade control loop of the SC, which controls both plasma shape and current. The simulation solver ode23tb was used, with relative tolerance 10^{-5}.

The scheme allows the simulation of vertical displacement events (VDE) that are considered as the primary benchmark of the disturbance-rejection performance. It also allows the simulation of different types of disturbances (minor disruptions, edge-localized-modes, L-H and H-L transitions), by injecting recorded profiles of β_p and l_i [4].

3. Shape controller

The plasma current and shape control algorithm described by Ariola and Pironti [5] has been implemented in the SC and it has been used in all the simulations. The SC output is the vector of the 11 main power supply voltages $\mathbf{V}_{\mathrm{PF}}$. The SC inputs are:
- the vector of controlled gaps **g**, comprising two strike-points and four gaps (see [5]),
- the plasma current I_p,
- the currents in the 11 superconductive coils $\mathbf{I}_{\mathrm{PF}}$.

The SC implements a multivariable proportional-integral control law for **g** and I_p, with an additional proportional contribution from $\mathbf{I}_{\mathrm{PF}}$.

4. Vertical stabilisation

The main aim of this paper is to compare different choices for the VS control algorithm, and to assess their impact on the performance of the SC described in the previous section. Four different algorithms are considered for VS; all of them act on the same control variables $\mathbf{u}_{\mathrm{VS}} = [u_{\mathrm{VS},1}\, u_{\mathrm{VS},2}]^{\mathrm{T}}$, where:
- $u_{\mathrm{VS},1}$ is the voltage applied to the IV coils VS3,
- $u_{\mathrm{VS},2}$ is the voltage applied to the SC circuit VS1.

In the following more details about the four considered algorithms are given.

4.1 Static output feedback (SOF)

The first considered option for the VS control algorithm is the SOF originally introduced in [4,10], which controls $\mathbf{y}_{\mathrm{VS}} = [y_{\mathrm{VS},1}\, y_{\mathrm{VS},2}]^{\mathrm{T}}$, where:
- $y_{\mathrm{VS},1}$ is the current in the IV coils IVS3,
- $y_{\mathrm{VS},2}$ is the plasma vertical velocity v_p.

In this paper the following static gain matrix is used

$$\mathbf{u}_{\mathrm{VS}}(t) = \mathbf{K}_{\mathrm{SOF}}\mathbf{y}_{\mathrm{VS}}(t), \quad \mathbf{K}_{\mathrm{SOF}} = \begin{bmatrix} 0.0108 & -1200 \\ 0.1 & 0 \end{bmatrix} \tag{1}$$

4.2 SOFz

The SOFz VS controller controls also the plasma position z_p. An additonal gain from $y_{\mathrm{VS},3} = z_p$ to VS1 = $u_{\mathrm{VS},2}$ is added:

$$\mathbf{u}_{\mathrm{VS}}(t) = \mathbf{K}_{\mathrm{SOFz}}\mathbf{y}_{\mathrm{VS}}(t), \quad \mathbf{K}_{\mathrm{SOFz}} = \begin{bmatrix} 0.0108 & -1200 & 0 \\ 0.1 & 0 & -10000 \end{bmatrix} \tag{2}$$

4.3 Continuous-time LQG (ctLQG)

The ctLQG controller [6] is designed with a third-order nominal model $\{\mathbf{A}_r, \mathbf{B}_r, \mathbf{C}_r, \mathbf{0}\}$, obtained from the model LMVS via Schur balanced truncation [11], and the folowing tuning parameters for the LQ controller:

$$\mathbf{Q}_{\mathbf{y}} = \begin{bmatrix} 0.00001 & 0 \\ 0 & 1 \end{bmatrix}, \quad \mathbf{R}_{\mathbf{u}} = \begin{bmatrix} 0.008 & 0 \\ 0 & 0.0001 \end{bmatrix} \tag{3}$$

and the Kalman filter (KF):

$$\mathbf{Q}_{KF,\mathbf{y}} = \mathbf{B}_r\mathbf{B}_r^T, \quad \mathbf{R}_{KF,\mathbf{u}} = \begin{bmatrix} 0.001 & 0 \\ 0 & 10^{-13} \end{bmatrix} \tag{4}$$

4.4 ctLQGz

The ctLQGz controller is based on the ctLQG. The additional control loop from z_p is implemented by augmenting the nominal model with an integrator

$$\mathbf{A}_a = \begin{bmatrix} \mathbf{A}_r & \mathbf{0}_{3\times1} \\ \mathbf{C}_{r,2} & 0 \end{bmatrix}, \quad \mathbf{B}_a = \begin{bmatrix} \mathbf{B}_a \\ \mathbf{0}_{2\times1} \end{bmatrix}, \quad \mathbf{C}_a = \begin{bmatrix} \mathbf{C}_r & \mathbf{0}_{2\times1} \\ \mathbf{0}_{1\times3} & 1 \end{bmatrix} \tag{3}$$

where $\mathbf{C}_r^T = \begin{bmatrix} \mathbf{C}_{r,1}^T & \mathbf{C}_{r,2}^T \end{bmatrix}$. The additional diagonal element of the controller output cost matrix $\mathbf{Q}_{\mathbf{y}}$ is set equal to $2 \cdot 10^2$, and the additional diagonal elements of the KF covariance matrices for the input $\mathbf{R}_{\mathrm{KF}}$ and the state $\mathbf{Q}_{\mathrm{KF}}$ are equal to 10^{-15} and 1, respectively.

5. Simulation results

Simulation results for VDE events with the initial amplitude –0.1 m with different local models and controllers are given in Table 2 and Figs. 1-8.

Table 2 lists RISE values of the main process signals in simulations using the same SC with the four different VS controllers, and with five different local models in order to roughly assess the sensitivity of the schemes to the varying operating conditions. The RISE values are computed from the equilibrium point of the linear model, for the time interval from 0 s to 25 s.

Figs. 1-8 show display the main process signals simulated in the same time interval. Figs. 1-4 display the simulation of the four control schemes with LMNE, and Figs. 5-8 with LM52, respectively. All graphs show "delta" signal values (i.e., the deviations from the equilibrium operating point of the linear model).

Comparing the SOF and ctLQG simulations, especially with LMNE, the ctLQG shows a much more oscillatory response initially. But it should be pointed out that the ctLQG is designed in the LMVS operating point and manages to retain stability in the substantially different operating point of LMNE. The SOF parameters

for the LMVS model [4,10] result in an unstable response with LMNE. On longer term, comparing the responses of the controlled gaps, the ctLQG manages to decrease the peak values of gap overshoots after the disturbances. This is most likely because ctLQG immediately acts with both actuators VS3 and VS1 after the disturbance, while with SOF the action of VS1 is slightly delayed.

The implementation of the additional control loop that brings z_p to zero, acting on a slower time-scale than the VS but faster than the SC, shows a further improvement in the suppression of the transients after the VDE, both with the SOF and the ctLQG, and works robustly with different local models.

6. Conclusion

The simulated VDE responses show an obvious improvement in the suppression of disturbances. This indicates that there is a considerable potential for faster and also more robust suppression of VDE disturbances, compared to the plasma magnetic control schemes proposed for the ITER tokamak in [4] and [10]. However, best implementation and integration with the SC layer is yet to be explored.

Acknowledgments

This work was carried out in collaboration with Cosylab, d.d., and was supported by the Competence Centre for Advanced Control Technologies, partly financed by the Republic of Slovenia, Ministry of Education, Science, Culture and Sport, and European Union, European Regional Development Fund.

References

[1] T. Bellizio et al., Control of elongated plasma in presence of ELMs in the JET tokamak, IEEE T. Nucl. Sci. **58**, 4 (2011)

[2] A. Neto et al., Exploitation of Modularity in the JET Tokamak VS System, Control Eng. Pract. **20**, 9 (2012)

[3] G. Ambrosino et al., Design of the Plasma Position and Shape Control in the ITER Tokamak Using In-Vessel Coils, IEEE Trans. Plasma Science **37** (2009)

[4] G. Ambrosino et al., Plasma Vertical Stabilization in the ITER Tokamak via Constrained Static Output Feedback, IEEE T. Contr. Syst. T. **19**, 2 (2011)

[5] M. Ariola and A. Pironti, An Application of the Singular Perturbation Decomposition to Plasma Position and Shape Control, Eur. J. Control **9** (2003) 410–420

[6] S. Gerkšič and G. De Tommasi, Vertical stabilization of ITER plasma using explicit model predictive control, Fusion Engineering and Design, (2013), in press, http://dx.doi.org/10.1016/j.fusengdes.2013.02.021

[7] D. A. Ovsyannikov et al., Mathematical methods of plasma vertical stabilization in modern tokamaks, Nuclear Fusion **46** (8) (2006) S652–S657

[8] R. Albanese and F. Villone, The linearized CREATE-L plasma response model for the control of current, position and shape in tokamaks, Nucl. Fus. **38** (5) (1998)

[9] R. Albanese et al., Plasma response models for current, shape and position control at JET, Fusion Eng. Des. **66–68** (2003)

[10] G. Ambrosino et al., Robust vertical control of ITER plasmas via static output feedback, Proc. IEEE MSC'11, Denver CO (2011)

[11] M. G. Safonov and R. Y. Chiang, A Schur Method for Balanced Model Reduction, IEEE T. Automat. Contr. **34**, 7, (1989)

Table 2. RISE values (from the equilibrium values).

VDE-LMNE	SOF	SOFz	ctLQG	ctLQGz
max(RISE(**g**))	0.12954	0.10395	0.07920	0.07322
avg(RISE(**g**))	0.03682	0.02872	0.02281	0.02092
max(RISE($\mathbf{g}_{all}$))[1]	0.17274	0.13706	0.1053	0.09702
avg(RISE($\mathbf{g}_{all}$))	0.03310	0.02539	0.02054	0.01875
RISE(IVS3)	33706	33993	36925	36357
RISE(IVS1)	2359.2	1745.3	1471	1344.2
RISE(VS3)	70.241	70.488	98.25	97.126
RISE(VS1)	2434.5	2444.2	3359.4	3283.2
RISE(v_p)	0.36826	0.37008	0.61302	0.60184
RISE(z_p)	0.04889	0.03738	0.03050	0.02783
RISE(I_p)	55348	41547	34345	31177
VDE-LM52	SOF	SOFz	ctLQG	ctLQGz
max(RISE(**g**))	0.23264	0.17479	0.16212	0.13224
avg(RISE(**g**))	0.08229	0.06065	0.05863	0.04727
max(RISE($\mathbf{g}_{all}$))	0.46313	0.32328	0.31596	0.24904
avg(RISE($\mathbf{g}_{all}$))	0.10914	0.07632	0.07644	0.06047
RISE(IVS3)	19540	21728	10063	9840.8
RISE(IVS1)	6923.2	3578.4	5323.6	4097.4
RISE(VS3)	187.69	200.37	157.14	156.92
RISE(VS1)	1952.1	1209.8	2534.3	2435.7
RISE(v_p)	0.11797	0.11813	0.12949	0.13179
RISE(z_p)	0.17024	0.1221	0.11901	0.09539
RISE(I_p)	216690	131650	172240	134900
VDE-LM53	SOF	SOFz	ctLQG	ctLQGz
max(RISE(**g**))	0.20278	0.15679	0.1337	0.11235
avg(RISE(**g**))	0.07587	0.05621	0.05183	0.04289
max(RISE($\mathbf{g}_{all}$))	0.54276	0.3838	0.3511	0.28416
avg(RISE($\mathbf{g}_{all}$))	0.11282	0.07956	0.07518	0.06094
RISE(IVS3)	20949	23110	12019	11860
RISE(IVS1)	7615.1	4125.7	5486.8	4311.1
RISE(VS3)	217.33	227.73	192.37	192.27
RISE(VS1)	2091.9	1378.5	2659.4	2586.5
RISE(v_p)	0.15468	0.15364	0.16306	0.16504
RISE(z_p)	0.15947	0.1181	0.10606	0.08749
RISE(I_p)	206700	123140	155420	122600
VDE-LM59	SOF	SOFz	ctLQG	ctLQGz
max(RISE(**g**))	0.29556	0.2029	0.22144	0.16562
avg(RISE(**g**))	0.10564	0.06922	0.08093	0.05993
max(RISE($\mathbf{g}_{all}$))	0.53418	0.35555	0.38746	0.28263
avg(RISE($\mathbf{g}_{all}$))	0.13106	0.08540	0.09791	0.07147
RISE(IVS3)	19248	20042	9091	8624.3
RISE(IVS1)	5783.8	2643.2	4817.6	3459
RISE(VS3)	160.87	165.85	133.89	132.64
RISE(VS1)	1924.2	1054.6	2693	2533.1
RISE(v_p)	0.06481	0.06427	0.10117	0.10228
RISE(z_p)	0.21049	0.13554	0.15832	0.11635
RISE(I_p)	290750	181330	251910	192320
VDE-LM60	SOF	SOFz	ctLQG	ctLQGz
max(RISE(**g**))	0.31643	0.2205	0.23024	0.17821
avg(RISE(**g**))	0.10723	0.07581	0.07879	0.06082
max(RISE($\mathbf{g}_{all}$))	0.55091	0.36274	0.39147	0.29641
avg(RISE($\mathbf{g}_{all}$))	0.13219	0.08986	0.09583	0.07296
RISE(IVS3)	19519	21021	8368.1	7989.6
RISE(IVS1)	6956.2	3315.1	5597.6	4168.2
RISE(VS3)	171.76	182.55	117.14	116.17
RISE(VS1)	1950.9	1147.6	2395.5	2248.4
RISE(v_p)	0.08810	0.08931	0.09814	0.10036
RISE(z_p)	0.18832	0.1287	0.13733	0.10566
RISE(I_p)	178030	110680	153100	120170

[1] $\mathbf{g}_{all}$ is the vector of two strike-points and all of the 26 to 43 gaps, as defined in different local models. RISE values of $\mathbf{g}_{all}$ may therefore not be compared across different local models.

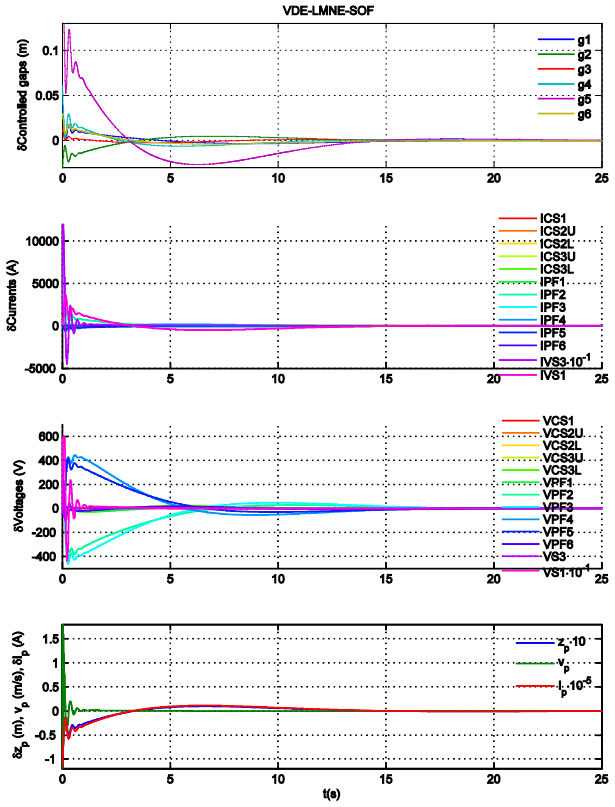

Fig. 1. 10 cm VDE simulation: SOF, model LMNE.

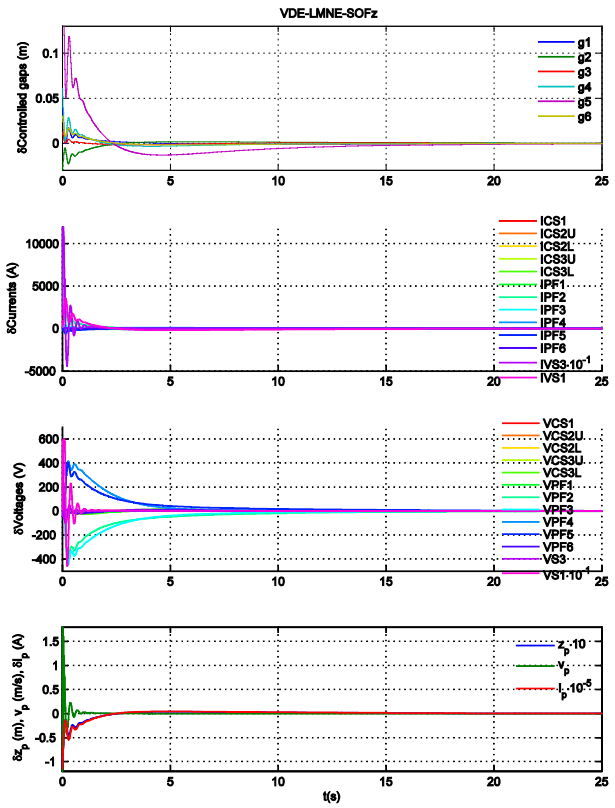

Fig. 2. 10 cm VDE simulation: SOFz, model LMNE.

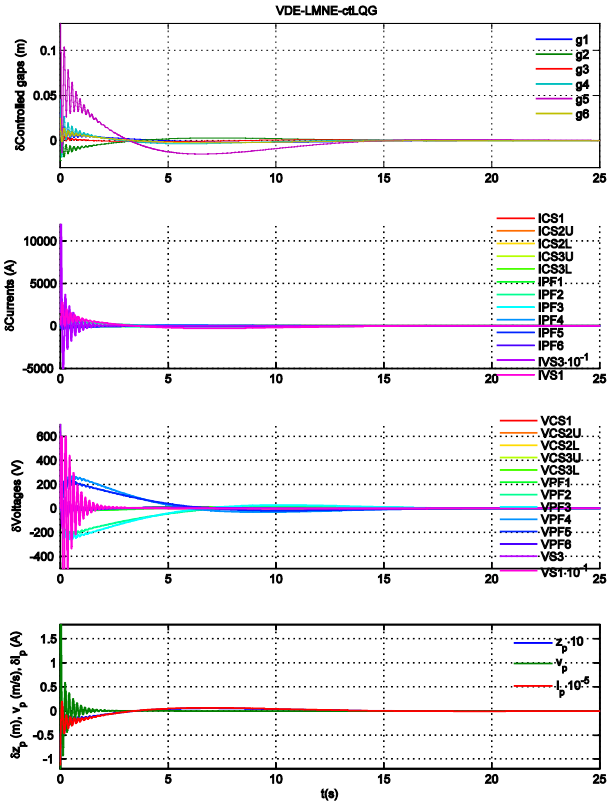

Fig. 3. 10 cm VDE simulation: ctLQG, model LMNE.

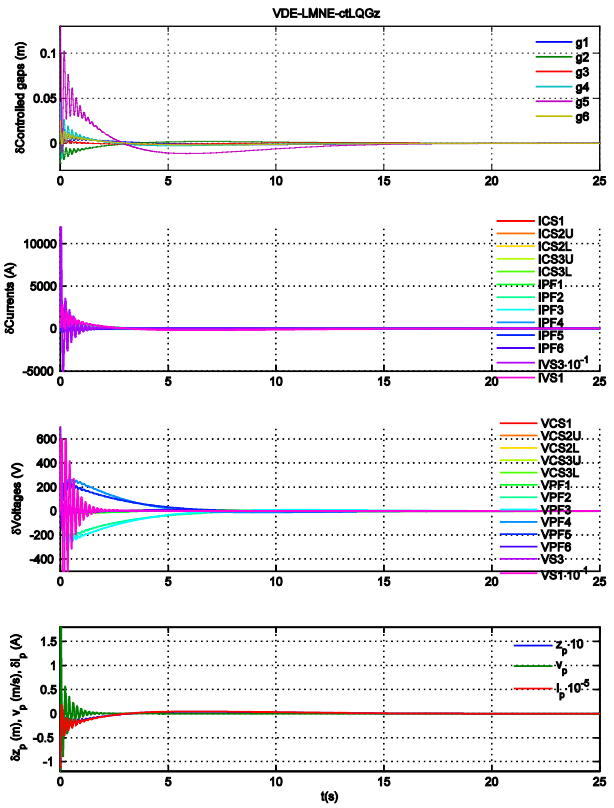

Fig. 4. 10 cm VDE simulation: ctLQGz, model LMNE.

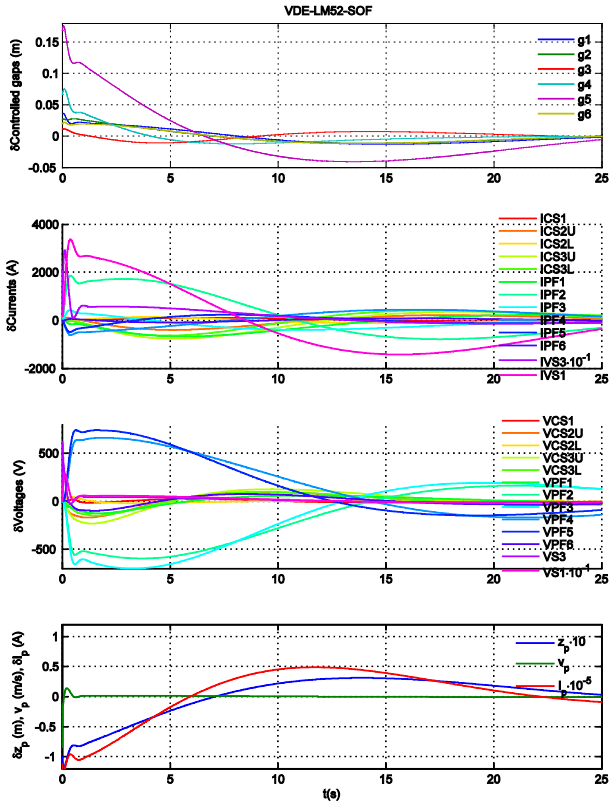

Fig. 5. 10 cm VDE simulation: SOF, model LM52.

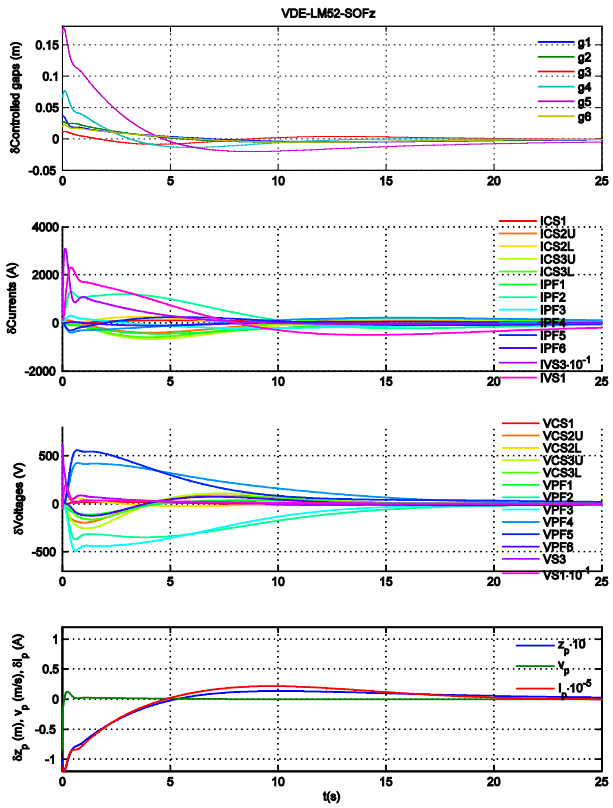

Fig. 6. 10 cm VDE simulation: SOFz, model LM52.

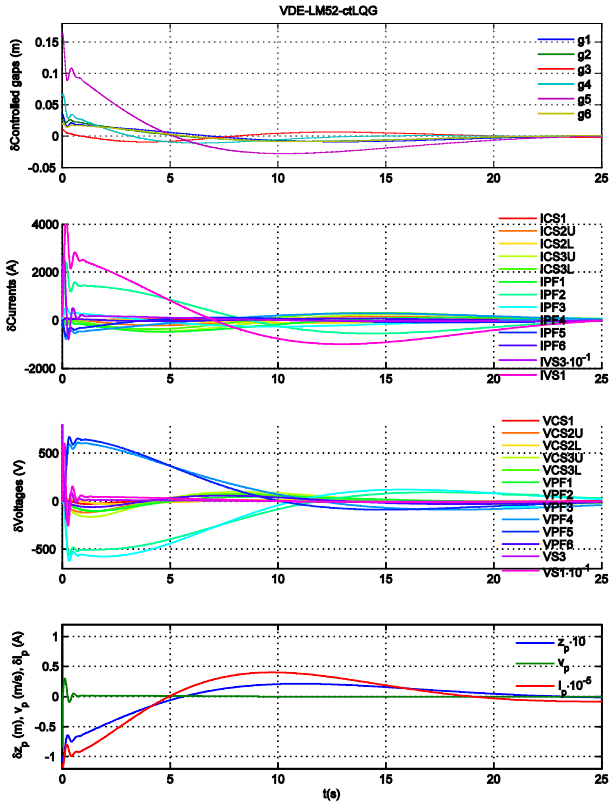

Fig. 7. 10 cm VDE simulation: ctLQG, model LM52.

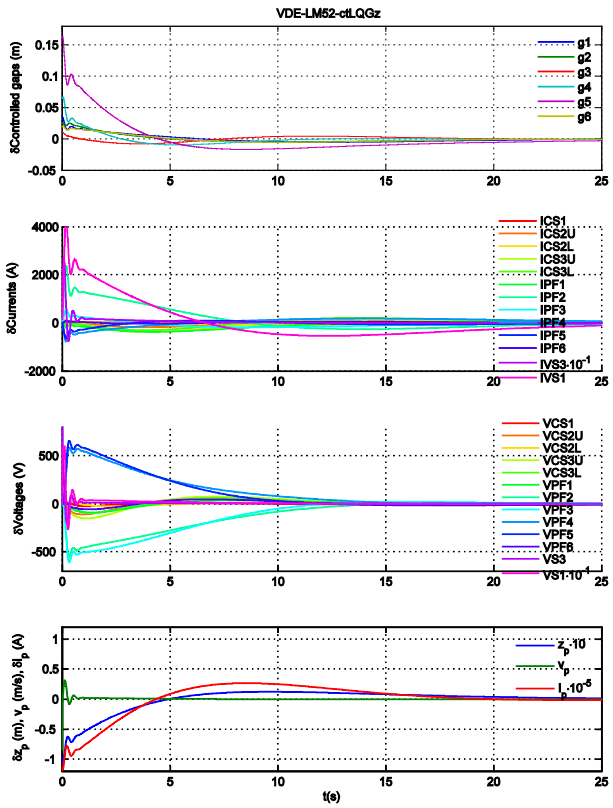

Fig. 8. 10 cm VDE simulation: ctLQGz, model LM52.